

## Supplementary Material

### Deliquescence, Efflorescence, and Phase Miscibility of Mixed Particles of Ammonium Sulfate and Isoprene-Derived Secondary Organic Material

M.L. Smith, A.K Bertram, and S.T. Martin

#### S1. The optimal value of $RH^{\text{mono}}$ for transmission ratio measurements

A goal of our experiments was to probe a maximum range of organic volume fractions  $\varepsilon$  while ensuring  $g > 1.12$ . For this purpose there existed an optimal value of  $RH^{\text{mono}}$ . A requirement of the deliquescence mode experiments was that the particles must not yet be fully deliquesced at  $RH^{\text{mono}}$ . In this regard, a low value of  $RH^{\text{mono}}$  avoided full deliquescence to some high value of  $\varepsilon$ . A high value of  $RH^{\text{mono}}$ , however, favored compliance with the condition  $g > 1.12$ . The optimal value of  $RH^{\text{mono}}$  was the value that just satisfied  $g = 1.12$  while maximizing  $\varepsilon$  (cf. Fig. S2). A priori to our collected data set, the optimal value of  $RH^{\text{mono}}$  could not be known, but the results of initial survey experiments conducted by us suggested a good value for  $RH^{\text{mono}}$  would be 60% for the deliquescence mode experiments, and this value was used in collecting the detailed data set. Similarly, for the efflorescence mode experiments, initial survey experiments established that  $RH^{\text{mono}}$  of 50% was a good value, and this value was used to collect the detailed data sets. A posteriori to the collection of the data set, the optimal value could be established as 69.5% for both the deliquescence and efflorescence mode experiments, corresponding to a maximum range of  $0 < \varepsilon < 0.66$  that could possibly be measured in a transmission ratio experiment (cf. Fig. S2).

## S2. Connection between phase miscibility gap and transmission ratio experiments

Transmission ratios for efflorescence experiments were modeled to determine whether our data were consistent with a gap in phase miscibility that extended to RH above the curve  $ERH(\varepsilon)$ . For aqueous particles of  $d_{m,+1}^{mono} = 90$  nm,  $P(\varepsilon)$  and the parameterized curve  $ERH(\varepsilon)$  were used to model the transmission ratio response (i.e., as RH is decreased, the drop in transmission ratio at any RH is proportional to the fraction of particles in the population that have an  $ERH \geq$  that RH). In Fig. S6, the miscibility gaps investigated (panels a - c) and the corresponding modeled transmission ratios (panels d -f) are shown. Also plotted in panels d – f is the measured transmission ratio. For the case of fully miscible phases (Fig. S6a and d), the modeled drop in transmission ratio is continuous and smoothly decreases with decreasing RH. This transmission ratio response matches the measured data well. For the cases of a miscibility gap (Fig. S6b/e and c/f), tie lines that define the composition of each phase can be drawn between  $ERH(\varepsilon)$  and the miscibility gap boundary. For decreasing RH, at the point that the miscibility gap boundary and  $ERH(\varepsilon)$  first intersect, one of the phases in a phase-separated particle is necessarily of a composition that induces particle efflorescence at that RH (i.e., as defined by a tie line). The absence of a discontinuity in the data implies no large miscibility gap is present.

Equation	Experiment Label	$d_{m,+1}^{mono}$	$d_{m,+1}^{filter}$	Arm	$RH^{CMFR}$	$RH^{mono}$	$RH_1^{nafion}$	$RH_2^{nafion}$	Measurement
n/a	Deliquescence: Reference Arm	{75,120}	$d_{m,+1}^{mono}$	$\alpha$	40	60	60	60	$\frac{N_{\beta}^{filter}}{N_{\alpha}^{filter}}$
1	Deliquescence: Test Arm	{75,120}	$d_{m,+1}^{mono}$	$\beta$	40	60	x:60→90	60	$\frac{N_{\beta}^{filter}}{N_{\alpha}^{filter}}$
n/a	Efflorescence: Reference Arm	{90*,120*}	$d_{m,+1}^{mono}$	$\alpha$	40	50	50	50	$\frac{N_{\beta}^{filter}}{N_{\alpha}^{filter}}$
2	Efflorescence: Test Arm	{90*,120*}	$d_{m,+1}^{mono}$	$\beta$	40	50	x:50→15	50	$\frac{N_{\beta}^{filter}}{N_{\alpha}^{filter}}$
3a	Hygroscopic Test for Deliquescence	{75,190}	scanned	$\beta$	40	7	x:10→85	x:10→85	$N(d)$
3b	Hygroscopic Control for forced Deliquescence	{75,190}	scanned	$\beta$	40	7	90	x:10→85	$N(d)$
5a	Hygroscopic Test for Efflorescence at 7%	{75,150}	scanned	$\beta$	40	7	50	50	$N(d)$
5b	Hygroscopic Test for Efflorescence at 7%	{75,150}	scanned	$\beta$	40	7	90	50	$N(d)$
n/a	Hygroscopic Test for Efflorescence - perturbation	{90*,120*}	scanned	$\beta$	40	50	x:50→9	50	$N(d)$

**Table S1.** List of experimental modes of TDMA operation and relative humidity cycles used to determine DRH( $\varepsilon$ ) and ERH( $\varepsilon$ ) from transmission ratio (rows 1-4) and number-diameter distribution experiments (rows 5-9). An asterisk (\*) indicates that the classified particle was on the upper branch of the hysteresis curve. Numbers enclosed in brackets (e.g., {75,120}) indicate that several values in-between these two numbers were studied.

$N_{3b}(d,y)$ compared to $N_{3a}(d,y)$ is...	$DRH(\varepsilon) > 40\%$	$ERH(\varepsilon) > 7\%$	$DRH(\varepsilon) > y$	$ERH(\varepsilon) > y$
n/a	True	True	True	<b>True</b>
shifted right	True	True	True	False
n/a	True	True	False	<b>True</b>
identical	True	True	False	False
n/a	True	False	True	<b>True</b>
shifted right	True	False	True	False
n/a	True	False	False	<b>True</b>
identical	True	False	False	False
n/a	False	True	True	<b>True</b>
n/a	<b>False</b>	True	<b>True</b>	False
n/a	False	True	False	<b>True</b>
identical	False	True	False	False
n/a	False	False	True	<b>True</b>
n/a	<b>False</b>	False	<b>True</b>	False
n/a	False	False	False	<b>True</b>
identical	False	False	False	False

**Table S2.** Evaluation of the 16 possible outcomes of the comparison of  $N(d,y;\varepsilon)$  of Eq. (3a) to that of  $N(d,y;\varepsilon)$  of Eq. (3b) based on whether the following conditions are true:  $DRH(\varepsilon) > 40\%$ ,  $ERH(\varepsilon) > 7\%$ ,  $DRH(\varepsilon) > y$ , and  $ERH(\varepsilon) > y$ . The entry “n/a” indicates a condition that, based on inference from the results of the transmission ratio experiments as summarized in Fig. 4, is never satisfied for this data set for  $y \geq 40\%$ . Bolded entries show the conditions that lead to “n/a”.

$N_{3b}(d,y)$ compared to $N_{3a}(d,y)$ is...	$\text{DRH}(\varepsilon) > 40\%$	$\text{ERH}(\varepsilon) > 7\%$	$\text{DRH}(\varepsilon) > y$	$\text{ERH}(\varepsilon) > y$
shifted right	True	n/a	True	n/a
identical	True	n/a	False	n/a
identical	False	n/a	n/a	n/a

**Table S3.** Condensed results of the analysis in Table S2 following removal of “n/a” entries and logically identical elements. This table appears as Eq. (4) in the main text, with the substitution of  $\text{DRH}(\varepsilon) > 40\%$  by  $\varepsilon < \varepsilon_D(40\%)$ .

Quantity	Lower Bound	Central Value	Upper Bound
$d_{m,+1}^{seed}$	+ 1 nm	0 nm	- 1 nm
$d_{m,+1}^{mono}$	- 1 nm	0 nm	+ 1 nm
$d_{m,+1}^{filter}$	+ 1 nm	0 nm	- 1 nm
$RH_2^{nafion}$	- 1 %	0 %	+ 1 %
$RH_{1,\beta}^{nafion}$	- 1 %	0 %	+ 1 %

**Table S4.** Combinations of uncertainties in diameter and relative humidity used to determine overall uncertainty in DRH( $\epsilon$ ) and ERH( $\epsilon$ ) (Fig. 4). The uncertainties of the measurements listed in columns 2 - 4 were applied to the quantities listed in column 1, and the data were subsequently analyzed as described in the main text (cf. Section 3.2) to produce the lower and upper bounds on DRH( $\epsilon$ ) and ERH( $\epsilon$ ). The  $\pm 1$  nm and  $\pm 1\%$  RH uncertainties were combined with sign conventions correlated to maximize the total error in DRH( $\epsilon$ ) and ERH( $\epsilon$ ) (i.e., combining opposite signed errors in both  $d_{m,+1}^{mono}$  and  $d_{m,+1}^{filter}$  increases the change in the value of  $\epsilon_D$  determined from number-diameter distribution experiments compared to combining similarly signed errors). Table S5 presents numerical examples of the individual effects of these uncertainties on the obtained values of  $\epsilon_D$ .

Source of uncertainty	DRH( $\varepsilon$ ) point: (0.80,48%)	DRH( $\varepsilon$ ) point: (0.20,79%)
+ 1 nm $d_{m,+1}^{seed}$	- 0.04	- 0.01
- 1 nm $d_{m,+1}^{mono}$	- 0.09	- 0.02
+ 1 nm $d_{m,+1}^{filter}$	- 0.12	- 0.01

**Table S5.** Change in  $\varepsilon_D$  determined from number-diameter distribution measurements resulting from uncertainties in diameters. The first column lists the diameter uncertainties that lead to a negative change in  $\varepsilon_D$ . Columns two and three show the decrease in  $\varepsilon_D$  resulting from only the diameter uncertainty listed in the corresponding row of column one (i.e., for row one,  $d_{m,+1}^{seed}$  was increased by 1 nm while  $d_{m,+1}^{mono}$  and  $d_{m,+1}^{filter}$  were not perturbed). The lowest and highest DRH( $\varepsilon$ ) points of Fig. 4 are shown to highlight the different effects of each type of error: For DRH(0.80) = 48 %, uncertainty in  $d_{m,+1}^{filter}$  induces the largest error in  $\varepsilon_D$ , while for DRH(0.20) = 79%, the decrease of 1 nm in  $d_{m,+1}^{mono}$  is the largest source of error.

## List of Figures

**Figure S1.** Examples of the number-diameter distributions of the ammonium sulfate seed particles in the CMFR inflow (solid lines) and of the number-diameter distributions of the mixed organic-inorganic particles in the CMFR outflow (dotted lines). The distributions are scaled to a height of unity so that the features of the particle population exiting the chamber can be clearly seen. The two shown distributions were collected 10 months apart, demonstrating consistency of the experimental conditions.

**Figure S2.** Optimal value of  $RH^{mono}$  for transmission ratio experiments. For both deliquescence- and efflorescence-mode experiments, the optimal value of  $RH^{mono}$  satisfies  $g = 1.12$  while maximizing  $\varepsilon$ . The line of  $g = 1.12$  is drawn in green. The  $DRH(\varepsilon)$  curve of this study, as parameterized in Table 1, is drawn in blue. The intersection of the green line with the blue line is the optimal value for  $RH^{mono}$ . This value is 69.5% and corresponds to  $\varepsilon_D(69.5\%) = 0.66$ . Higher values of  $\varepsilon$  can be probed through the number-diameter distribution experiments.

As further explanation, horizontal red lines labeled 1, 2, and 3 are drawn at  $RH^{mono} = 69.5\%$  and at values above and below  $RH^{mono}$ . The solid portion of the red line corresponds to  $g > 1.12$  so that the transmission ratio experiments can be carried out. The dashed portion of the red line corresponds to  $g < 1.12$  so that full size separation is not achieved between  $DMA^{mono}$  and  $DMA_{\beta}^{filter}$ .

Lines 1, 2, and 3 demonstrate that  $RH^{mono}$  is the optimal value to maximize the experimental range of  $\varepsilon$  that can be studied in the transmission ratio experiments. For line 1 compared to

line 2, transmission ratio experiments are possible for the full range of  $\varepsilon$  but  $\varepsilon_2 > \varepsilon_1$ . For line 3 compared to line 2, transmission ratio experiments are no longer possible once line 3 intersects the line of  $g = 1.12$ . In this case,  $\varepsilon_2 > \varepsilon_3$ . The value of  $\varepsilon_2$  therefore represents the maximum value.

As a technical note, the value of  $g$  required for complete separation between  $\text{DMA}^{\text{mono}}$  and  $\text{DMA}_\beta^{\text{filter}}$  increases for increasing setpoint diameter because the width of the DMA transfer function broadens. The stated value of 1.12 holds for a setpoint diameter of 100 nm.

**Figure S3.** Illustration of reversible and irreversible fluctuations in diameter with relative humidity.

Partially dissolved ammonium sulfate can recrystallize without an activation barrier, whereas fully dissolved ammonium sulfate cannot recrystallize until the efflorescence relative humidity is reached. Key: Red, ammonium sulfate; green, SOM; blue, water.

**Figure S4.** Additional examples of (a) DRH( $\varepsilon$ ) curves derived from transmission ratio experiments and (b) associated modeled cumulative distribution functions  $P(\varepsilon)$  of organic volume fraction. The vertical dashed line shows the condition  $g = 1.12$ . The DRH( $\varepsilon$ ) curves are consistent with one another despite the large differences in underlying  $P(\varepsilon)$  among the three experiments. This consistency indicates high confidence in the data analysis.

**Figure S5.** Modeling hygroscopic growth and phase transitions for number-diameter distribution experiments (Eq. (3a)). Columns correspond to the progressive steps of RH history represented by Eq. (3a). Rows represent particle types A, B, C, and D (cf. Section 3.1). The heavy colored lines in column 3 correspond to the same colored lines shown in Fig. 3a. The

sum of these lines is the modeled size distribution for the entire particle population and appears as the red dashed line of Fig. 3a.

For clarity of presentation, the distributions in Fig. S5 are represented by discretized bars, and the bar widths are shown at increased coarseness compared to the actual model. The gradient of bar shading represents the fraction  $f$  of ammonium sulfate that is dissolved, as follows: (1) the scale bar is shown in uniform gradient from 0.0 to 1.0 in ten equally sized height steps and (2) the gradient in height steps at one diameter in one panel represents the relative fraction of particles having that value of  $f$ . For instance, for particle type A at 40% RH, the bar at 90 nm shows that most particles are characterized by  $0.0 \leq f < 0.1$ , followed by some particles of  $0.1 \leq f < 0.2$ . By comparison, at 7% RH all particles have  $0.0 \leq f < 0.1$ . Particles that are of  $f = 1$ , indicating that they are on the upper side of the hysteresis loop, are represented by red shading. The heterogeneity in particle water content at different diameters and RH, shown by the shading of  $f$ , demonstrates the need for a hygroscopic model that incorporates the distribution of  $f$  and the corresponding diameter growth to aid in the interpretation of data sets such as those represented in Fig. 3a.

In regard to column 1, a further note of explanation is that the shown distributions represent a subset of the polydisperse distribution that exits the CMFR. This subset corresponds to those particles that are subsequently selected by DMA<sup>mono</sup> set to  $d_{m,+1}^{mono} = 90$  nm at 7% RH (Eq. (3a)). Column 1 illustrates the phase state of the relevant particle sub-population in the CMFR outflow.

**Figure S6.** The influence of a miscibility gap on transmission ratio experiments. Panels a – c show possible regions of a gap in miscibility (blue hashed area in b and c) and the curve  $ERH(\varepsilon)$  (dashed black). Panels d – f show the measured (black) and modeled (green)  $\varphi$  associated with each phase diagram case represented to the left. A gap in miscibility causes a discontinuous drop in  $\varphi$  (panels b/e and c/f). The transmission ratio experiment modeled using the assumption of full miscibility agrees with the measurement (panels a/d). Inset in panel a shows  $P(\varepsilon)$  for  $d_{m,+1}^{mono} = 90$  nm.

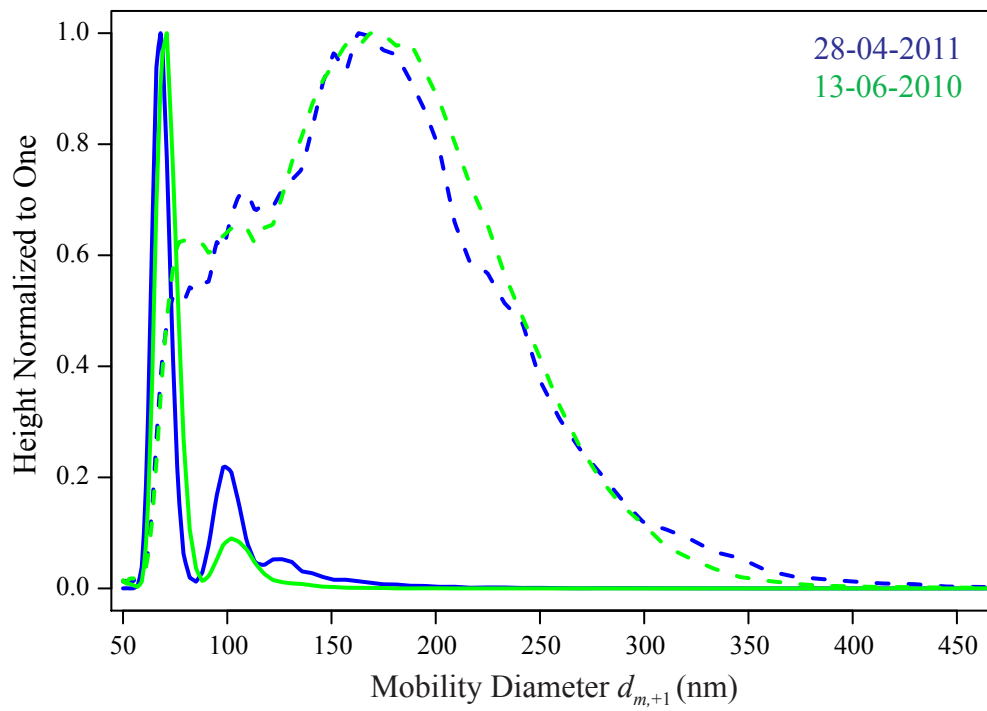
**Figure S7.** Correction made in the analysis for particle water content. Particles selected by  $DMA^{mono}$  for  $RH \geq 50\%$  contain non-negligible volumes of water; water-free distributions are needed to calculate  $P(\varepsilon)$ . An iterative optimization approach is used for estimating the dry number-diameter distribution, as follows: (1) a dry number-diameter distribution is assumed (panel a), (2) a model of hygroscopic growth is applied to the dry distribution (cf. Appendix of main text), and (3) the modeled distribution (solid lines, panel b) is compared to the distribution that is implied by the transfer function of  $DMA^{mono}$  (dashed line, panel b). These steps are repeated iteratively by refining the assumed dry number-diameter distribution and inputs to the hygroscopic growth model until the modeled distribution converges to the implied distribution. The optimized fraction of dissolved sulfate, which is unity at  $\varepsilon \geq \varepsilon_D$ , that was used to evolve the water-free distribution in panel A to the distribution at 64% RH in panel b is shown in the inset. Particle types A (blue), B (pink), and D (orange) are modeled separately. The cumulative distribution function given by  $P(\varepsilon) = \sum_T p(\varepsilon; T)$  appears in Figure 2b.

**Figure S8.** Hygroscopic diameter growth factors. (blue) The growth factor  $g_0$  of ammonium sulfate on the upper branch of the hysteresis curve is from Biskos et al. (2006). (red) The growth factor is unity for ammonium sulfate on the lower branch of the hysteresis curve. (green) The growth factor  $g_1$  of isoprene-derived SOM is parameterized as  $g_1(y) = 1 + (1 - y)^{-A} B y^C$  for  $A = 0.1683$ ,  $B = 0.1768$ ,  $C = 2.600$ , and  $y = \text{RH}/100$  for the data set shown in the inset for  $0.0 < y < 0.9$ . Horizontal dotted lines show the DRH and ERH of pure ammonium sulfate.

**Figure S9.** Sensitivity of (a)  $f(\varepsilon)$  and (b)  $p(d_{m,+1})$  to the value of parameter  $\varepsilon_D$ . The inset shows the sum of the squares of the differences between model predictions (lines) and data points (squares) for the different values of  $\varepsilon_D$  from 0.70 to 0.92. The specific values of  $\varepsilon_D$  for the lines correspond to the points shown in the inset (i.e., values of  $\varepsilon_D$  are more closely sampled near the minimum than away from it). In panels a and b, lines are colored from red (good fit) to blue (poor fit). The color bar is shown along the ordinate of the inset.

## References

Biskos, G., Paulsen, D., Russell, L. M., Buseck, P. R. and Martin, S. T.: Prompt deliquescence and efflorescence of aerosol nanoparticles, *Atmos. Chem. Phys.*, 6, 4633-4642, 2006.



" Figure S1

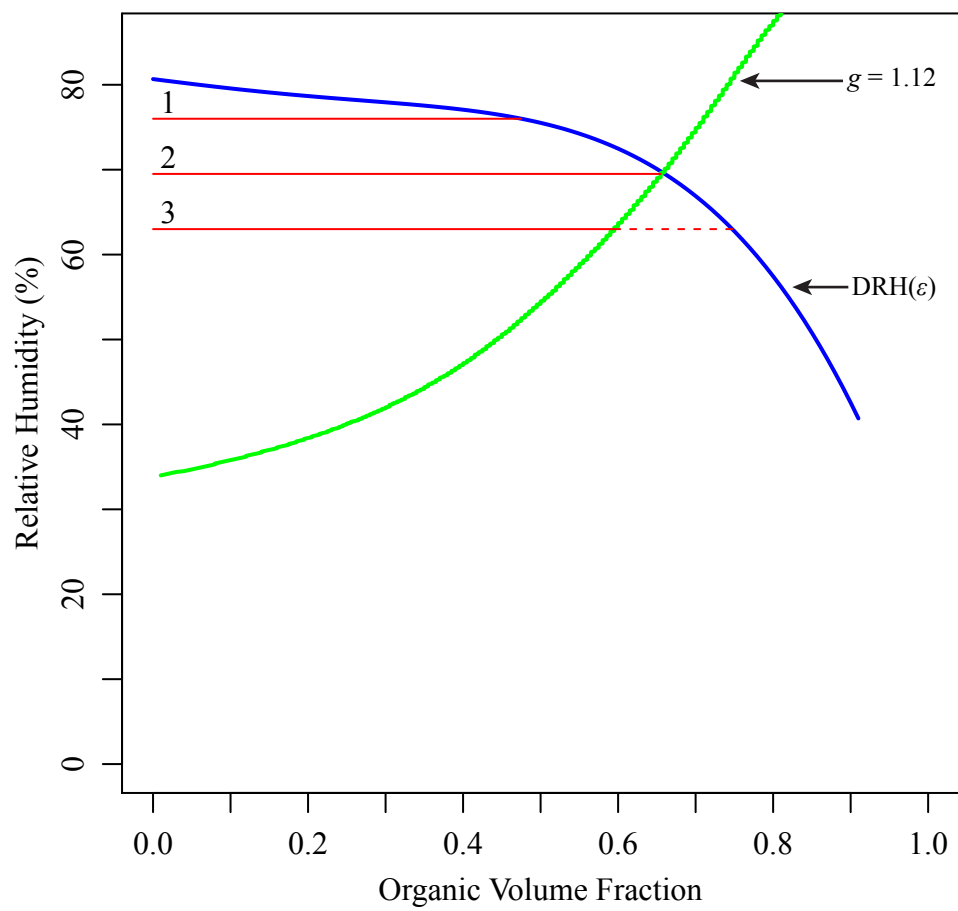


Figure S2

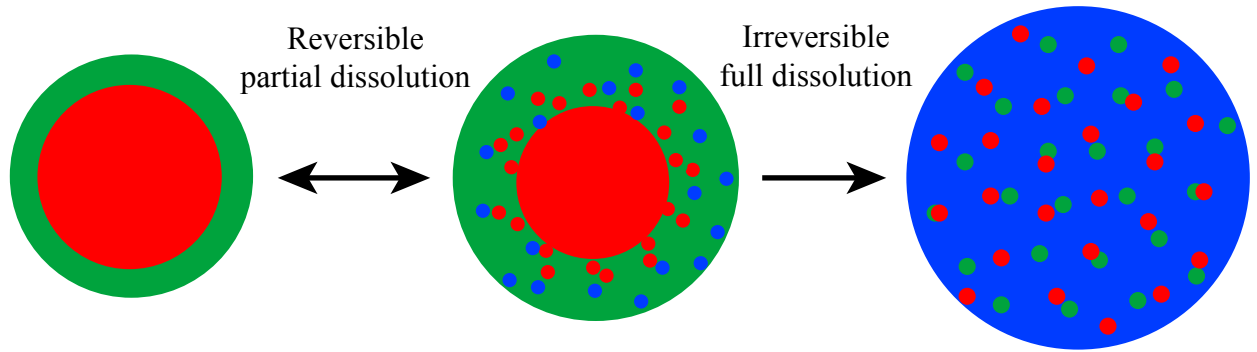


Figure S3

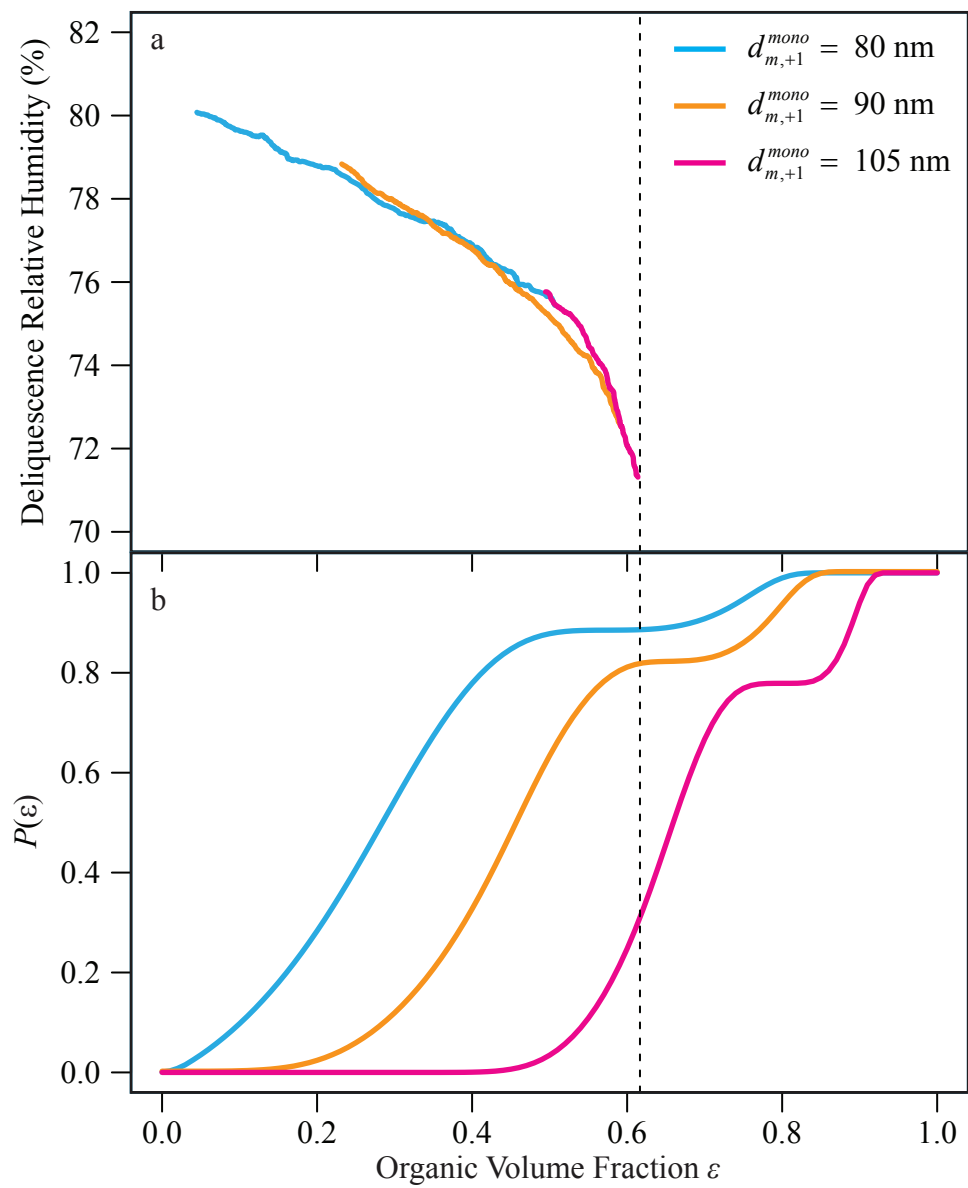


Figure S4

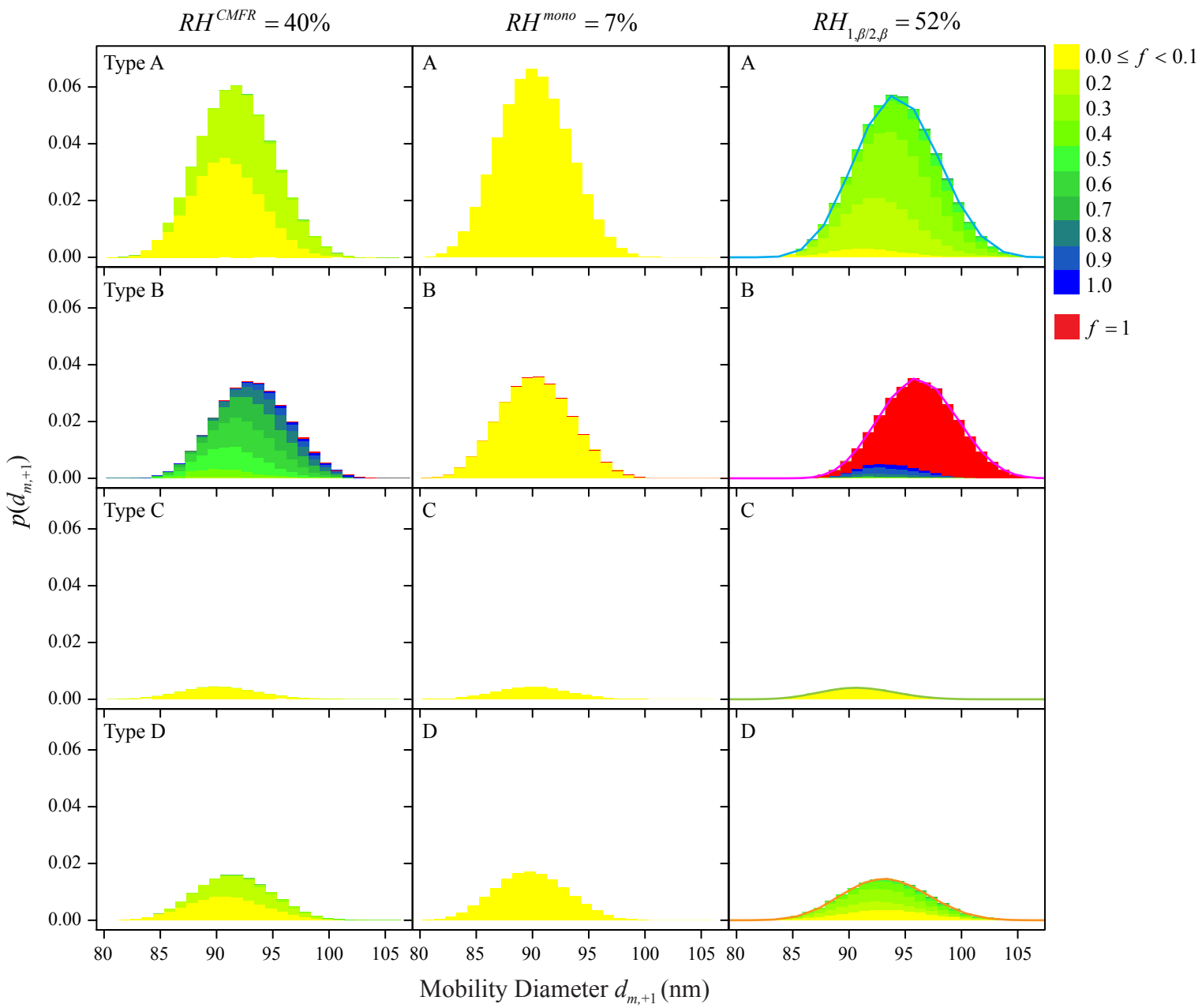


Figure S5

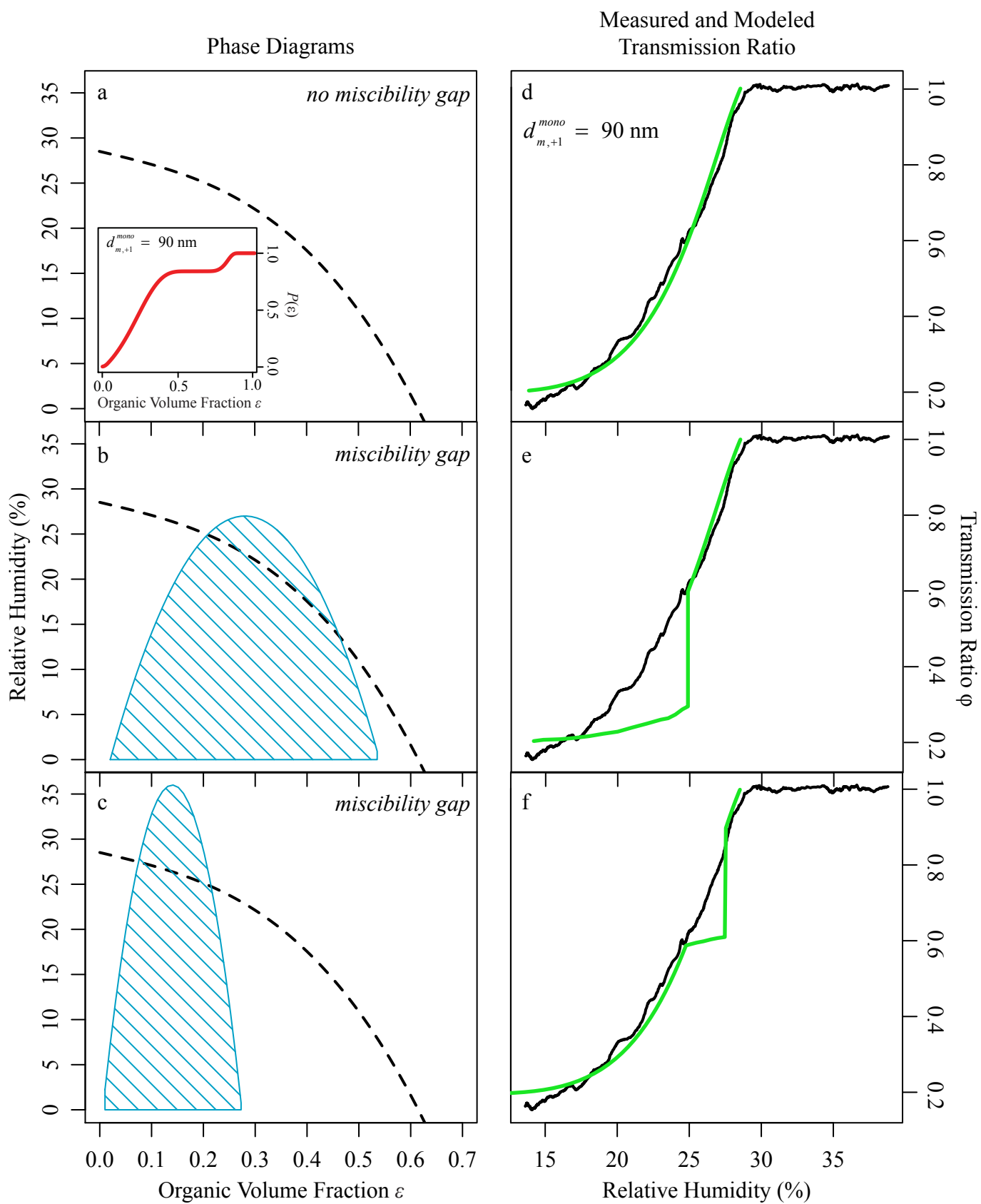


Figure S6

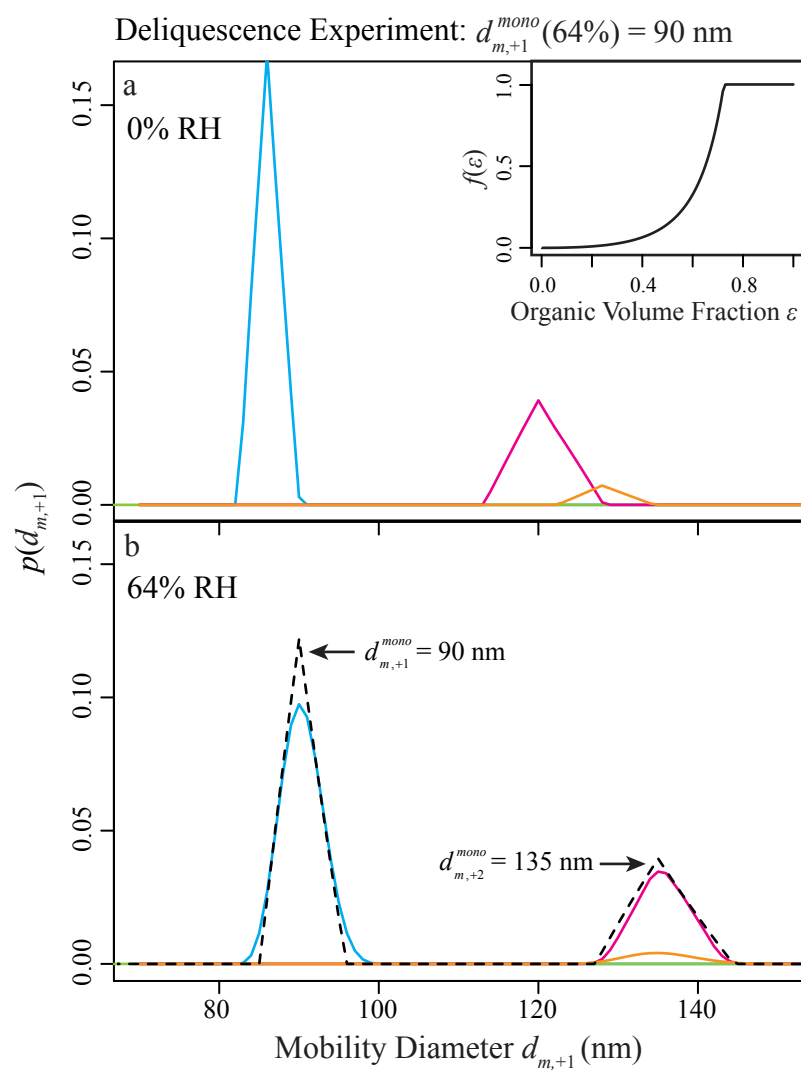


Figure S7

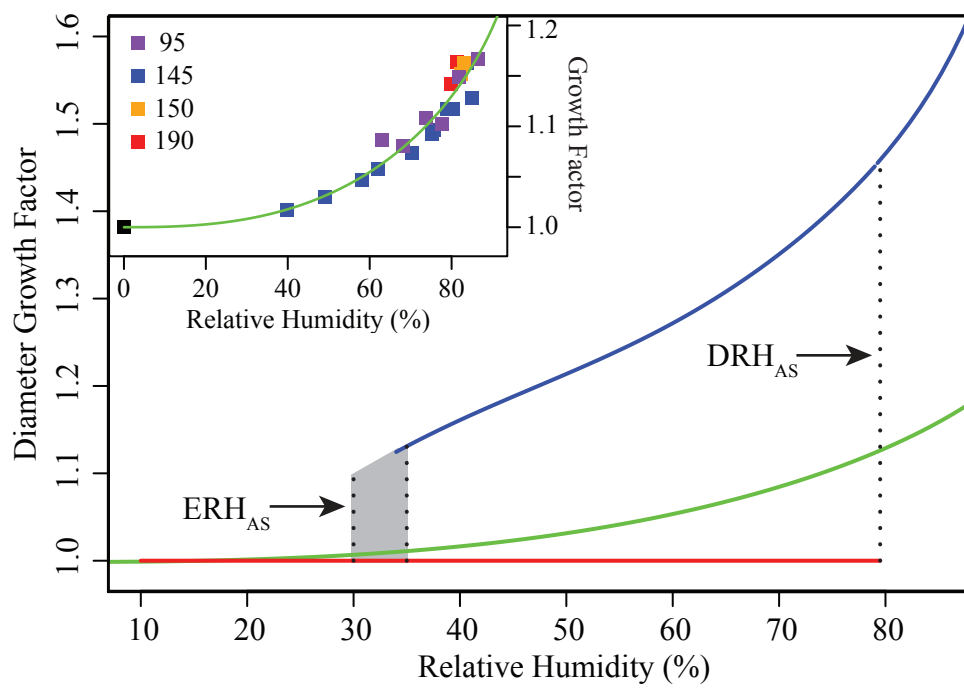


Figure S8

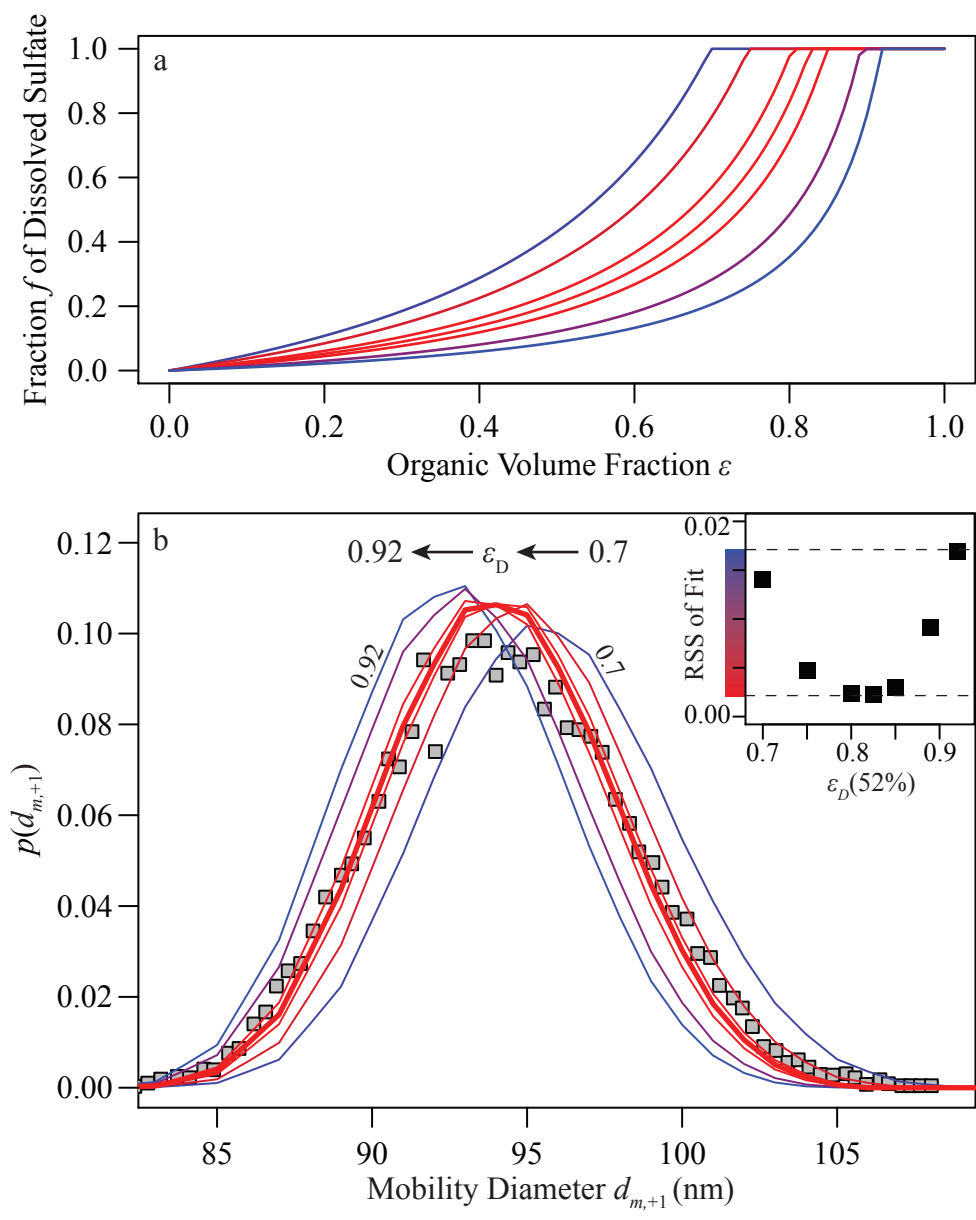


Figure S9